Population inversion study of GaAs/AlGaAs three-quantum-well quantum cascade structures

Jinlong Liu (刘金龙)[1*], Xiaoli Zhang (章小丽)[1], Jian Wang (王 健)[1], Yanwu Lü (吕燕伍)[1], and Suqing Duan (段素青)[2]

[1]*Department of Physics, School of Science, Beijing Jiaotong University, Beijing 100044, China*

[2]*Institute of Applied Physics and Computational Mathematics, Beijing 100088, China*

[*]*Corresponding author: Jeff_liu24@163.com*

Received November 2, 2012; accepted December 7, 2012; posted online March 28, 2013

A population inversion study of GaAs/$Al_xGa_{1-x}As$ three-quantum-well quantum cascade structures is presented. We derive the population inversion condition (PIC) of the active region (AR) and discuss the PICs on different structures by changing structural parameters such as the widths of quantum wells or barriers in the AR. For some instances, the PIC can be simplified and is proportional to the spontaneous emission lifetime between the second and the first excited states, whereas some other instances imply that the PIC is proportional to the state lifetime of the second excited state.

OCIS codes: 140.5965, 140.3070.

doi: 10.3788/COL201311.041409.

The quantum cascade laser (QCL) has become an important source of coherent radiation in the mid-infrared region, and its frequency range has been extended to the terahertz region[1]. The QCL currently exhibits excellent performance[2−7]. Theoretical research is an effective tool to facilitate laser fabrication[8]. In this letter, we study the mechanisms by which the widths of quantum wells (QWs) and barriers in the active region (AR) can affect the population inversion of QCL.

The time-independent Schrodinger equation of an electron with mass m in one-dimensional potential $V(x)$ is

$$\widehat{H}(x)\phi(x) = -\frac{\hbar^2}{2}\frac{\mathrm{d}}{\mathrm{d}x}\Big(\frac{1}{m}\frac{\mathrm{d}\phi}{\mathrm{d}x}\Big) + V(x)\phi(x) = E\phi(x), \quad (1)$$

where $V(x)$ includes $-eFx$, the potential caused by the applied electric field F, and e is the electron charge. To solve Eq. (1), the wave function and potential are discretized. $N+1$ points are selected to equally divide the AR, and the position coordinate of the electron can be expressed as $x_j = j\times h_0$, where h_0 is the step length, $j = 0, 1, 2,\cdots, N$, and $x_{j+1} = x_j + h_0$. The total length of the AR of the QCL is $L_\mathrm{a} = Nh_0$. At each selected point, the wave function and potential are $\phi_j = \phi(x_j)$ and $V_j = V(x_j)$, respectively. The first-order derivative of the discrete wave function at two adjacent points can be expressed in the finite difference approximation as $\frac{1}{m}\frac{\mathrm{d}\phi(x_j)}{\mathrm{d}x} = \frac{\phi(x_j)-\phi(x_{j-1})}{m_j h_0}$. To obtain the second-order derivative of the discrete wave function, three adjacent points must be considered, resulting in the following expression:

$$\frac{\mathrm{d}}{\mathrm{d}x}\Big(\frac{1}{m}\frac{\mathrm{d}\phi(x_j)}{dx}\Big) = \frac{1}{m_{j+1}h_0^2}[\phi(x_{j+1}) - \phi(x_j)] - \frac{1}{m_j h_0^2}[\phi(x_j) - \phi(x_{j-1})]. \quad (2)$$

After taking Eq. (2) into Eq. (1), we obtain the matrix equations of the AR:

$$(\mathbf{H} - E\mathbf{1})\phi(x) = \sum_{j=\mathbf{0}}^{N}\Big[-\mathbf{u}_j\phi(\mathbf{x}_{j-\mathbf{1}}) + (d_j - E)\phi(x_j) - u_{j+1}\phi(x_{j+1})\Big] = 0, \quad (3)$$

in which the Hamiltonian is a symmetric diagonal matrix, wherein $\mathbf{1}$ is the unit matrix, the diagonal matrix element is $d_j = \frac{\hbar^2}{2h_0^2}(\frac{1}{m_{j+1}} + \frac{1}{m_j}) + V_j$, and the adjacent non-diagonal matrix element is $u_j = \frac{\hbar^2}{2m_j h_0^2}$. Setting x_0 and x_N as the boundary coordinates of AR, the boundary conditions of the region are

$$\phi(x_0) = \phi(x_N), \quad (4)$$

$$\frac{1}{m_0}\frac{\mathrm{d}\phi}{\mathrm{d}x}\Big|_{x=x_0} = \frac{1}{m_N}\frac{\mathrm{d}\phi}{\mathrm{d}x}\Big|_{x=x_N}. \quad (5)$$

We also obtain the matrix equation of the AR:

$$(\mathbf{H} - E\mathbf{1})\phi = \begin{pmatrix} (d_1 - E) & -u_2 & 0 & . & . & -u_1 \\ -u_2 & (d_2 - E) & -u_3 & . & . & . \\ 0 & -u_3 & (d_3 - E) & . & . & . \\ . & . & . & . & . & . \\ . & . & . & -u_{N-1} & (d_{N-1} - E) & -u_N \\ -u_1 & . & . & . & -u_N & (d_N - E) \end{pmatrix} \begin{pmatrix} \phi(x_1) \\ \phi(x_2) \\ \phi(x_3) \\ . \\ \phi(x_{N-1}) \\ \phi(x_N) \end{pmatrix} = \mathbf{0}. \quad (6)$$

The solutions of the matrix equation yield the eigen energies and wave functions of the AR. In our calculations the electron density of the AR is sufficiently small that we can neglect Poisson's equation[9].

Research results show a high probability of rapid subband thermalization through electron–electron scattering processes[10]. For thermalized subbands, the emission process in the AR dominates the tunneling output, which is extremely fast that the density of electrons in the first subband shown in Fig. 1 is nearly zero. The rate equations for the AR are

$$\frac{\mathrm{d}N_3}{\mathrm{d}t} = \frac{J}{eL_\mathrm{a}} - \frac{N_3}{\tau_3}, \tag{7}$$

$$\frac{\mathrm{d}N_2}{\mathrm{d}t} = \frac{N_3}{\tau_{32}} - \frac{N_2}{\tau_2}, \tag{8}$$

where $N_i (N_i = 2, 3)$ is the electron concentration in the i-th subband and J is the electrical current density. $1/\tau_3 = 1/\tau_{32}+1/\tau_{31}$, where τ_3 is the state lifetime (SL) or relaxation time (RT) of the third subband, and τ_{32} and τ_{31} are the reciprocals of the spontaneous emission rate (SER) between the third subband and two other subbands in Fig. 1, respectively. The SL or RT of the second subband τ_2 satisfies $1/\tau_2 = 1/\tau_{21}+1/\tau_{\mathrm{op}}$, where τ_{21} is the reciprocal of the SER between the second subband and the first subband, τ_{op} is the reciprocal of the intersubband polar-optical-phonon (POP) scattering rate between the second and the first subbands. In other words, τ_{32}, τ_{31}, and τ_{21} are the RTs of spontaneous emissions and can be expressed as[11]

$$\frac{1}{\tau_{\mathrm{if}}} = \gamma_0^{\mathrm{3D}} \times \left|F_{\mathrm{i}\to\mathrm{f}}\right|, \tag{9}$$

where $\gamma_0^{\mathrm{3D}} = \frac{e^2 n w_0^2}{6\pi\varepsilon_0 m^* c^3}$ and

$$F_{\mathrm{i}\to\mathrm{f}} = \frac{2m^*(E_\mathrm{f} - E_\mathrm{i})}{\hbar^2}\left|Z_{\mathrm{i}\to\mathrm{f}}\right|^2, \tag{10}$$

where n is the refractive index, m^* is the electron effective mass, $\omega_0 = (E_\mathrm{i} - E_\mathrm{f})/\hbar$, where E_i and E_f are the eigen energies of the initial and final states of spontaneous emission, respectively, ε_0 is the vacuum permittivity, c is the light velocity, and $|Z_{\mathrm{i}\to\mathrm{f}}|$ is the dipole matrix element. τ_{op} is the intersubband POP scattering relaxation time (SRT) between the second and the first subbands. Based on D. Ahn and S. L. Chuang's work[12], τ_{op} can be expressed as

$$\begin{aligned}\frac{1}{\tau_{\mathrm{op}}} &= E_\mathrm{q}\frac{2e^2}{8\sqrt{2}\pi\hbar^2}\sqrt{\frac{m^*}{E_\mathrm{t}}}\left[\frac{1}{\varepsilon_0}\left(\frac{1}{\varepsilon_\infty} - \frac{1}{\varepsilon_\mathrm{s}}\right)\right](n_\mathrm{q}+1) \\ &\times \int_0^\pi \frac{1}{|\cos\phi|}\mathrm{d}\phi\bigg|_{\phi\neq\frac{\pi}{2}} \int_{x_0}^{x_N} \phi_1(z)\phi_2(z)\mathrm{d}z \int_{x_0}^{x_N} \phi_1(z') \\ &\times \phi_2(z')\mathrm{d}z'\left(e^{-\frac{\sqrt{8m^* E_t}}{\hbar}\cos\phi|z-z'|} + 1\right),\end{aligned} \tag{11}$$

where E_q is the energy of POP, $E_\mathrm{t} = \hbar^2 k_\mathrm{t}^2/2m^*$, k_t is the wave vector of the electron in the plane parallel to the QWs, and ε_∞ and ε_s are the optical and static dielectric constants, respectively. The phonon occupation number n_q is given by the Bose-Einstein distribution $n_\mathrm{q} = \{\exp[(\hbar\omega_\mathrm{q})/k_\mathrm{B}T] - 1\}^{-1}$, where k_B is the Boltzmann constant.

Supposing that the electric current J injects into the third subband without loss, then it can be obtained from Eqs. (7) and (8),

$$N_3 - N_2 = \frac{J}{eL_\mathrm{a}}\tau_3\left(1 - \frac{\tau_2}{\tau_{32}}\right), \tag{12}$$

which is the population inversion condition (PIC) of QCL.

As shown in Fig. 2, the widths of the four barriers are denoted as W_{B1}, W_{B2}, W_{B3}, and W_{B4}, and the widths of the three QWs are denoted as W_{W1}, W_{W2}, and W_{W3}. For component x, the electron effective masses of $\mathrm{Al}_x\mathrm{Ga}_{1-x}\mathrm{As}$ and GaAs are $m^*_{\mathrm{GaAs}} = (0.063 + 0.087x)m_0$ and $m^*_{\mathrm{AlGaAs}} = 0.063m_0$, respectively, where m_0 is the free-electron mass. The conduction band discontinuity at $\mathrm{Al}_x\mathrm{Ga}_{1-x}\mathrm{As}$/GaAs heterointerface is ΔE_c =0.79x eV, and the applied electric field is F = 10 kV/cm. If W_{B1}= 4 nm, W_{W1}=0.5 nm, W_{B2}=1 nm, W_{W2}=15.5 nm, W_{B3}=2 nm, W_{W3}= 3 nm, and W_{B4}=6.5 nm, then three subbands contribute to the performance of the AR. The three subbands are denoted as subband1, subband2, and subband3, and the corresponding eigen energies are marked as E_1, E_2, and E_3. The energy difference E_2–E_1 $\approx$ 35.4–(–0.39) = 35.79 meV is very close to the POP energy of the AR: $E_{\mathrm{op}} = E_{\mathrm{op-AlGaAs}}\frac{L_{\mathrm{AlGaAs}}}{L_\mathrm{a}} + E_{\mathrm{op-GaAs}}(1 - \frac{L_{\mathrm{AlGaAs}}}{L_\mathrm{a}}) \approx 35.79$ meV, where $E_{\mathrm{op-AlGaAs}}$ and $E_{\mathrm{op-GaAs}}$ are the POP energies of $\mathrm{Al}_x\mathrm{Ga}_{1-x}\mathrm{As}$ and GaAs, respectively, and $L_{\mathrm{op-AlGaAs}}$ and $L_{\mathrm{op-GaAs}}$ are total thicknesses of $\mathrm{Al}_x\mathrm{Ga}_{1-x}\mathrm{As}$

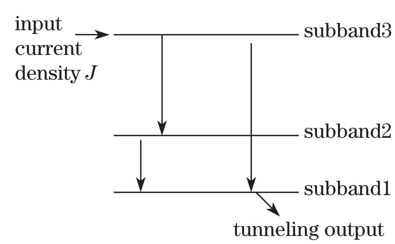

Fig. 1. Three-level diagram of the AR.

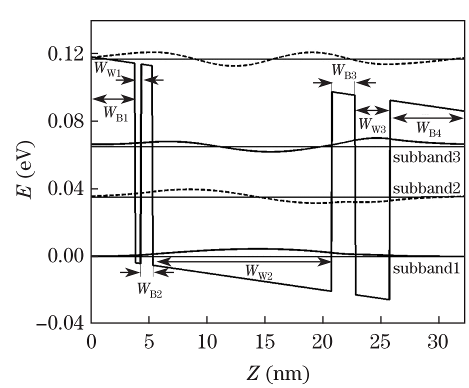

Fig. 2. Three-quantum-well AR, W_{B1} = 4 nm, W_{W1} = 0.5 nm, W_{B2} = 1 nm, W_{W2} = 15.5 nm, W_{B3} = 2 nm, W_{W3} = 3 nm, W_{B4} = 6.5 nm, and applied electric field F = 10 kV/cm.

and GaAs in the AR, respectively. The POP energy is $E_{\mathrm{op-AlGaAs}} = 36.25+1.83x+17.12x^2–5.11x^3$ meV, and $E_{\mathrm{op-GaAs}} = 35$ meV. The energy difference $E_3–E_2 = 64.9–35.4 = 29.5$ meV shows that the lasing wavelength (LW) is approximately 42.03 μm.

We set $E_{\mathrm{t}} = E_{\mathrm{op}}$ in calculating intersubband POP SRT. Setting W_{B1}=4 nm, W_{B2}=1 nm, W_{B3}=2 nm, and W_{B4}=6.5 nm, the spontaneous emission lifetimes (SELs) τ_{32}, τ_{31}, and τ_{21}, together with the POP SRT between subband2 and subband1 τ_{op}, and the LW of the QCL as functions of W_{W1}, W_{W2}, and W_{W3} were calculated. The calculation results are shown in Fig. 3. Setting W_{W1} as the linear variable, W_{W2} is changed correspondingly, and W_{W3} is changed slightly to make sure that $E_2–E_1 \approx E_{\mathrm{op}}$. The calculated values of W_{W1}, W_{W2}, and W_{W3} are listed in Table 1. Among the three SELs, τ_{31} has the longest time (Fig. 3(a)). When $\tau_{31} \approx$17.66 μs and $\tau_{32} \approx$0.69 μs, the ratio τ_{32}/τ_{31} has the maximum value 0.039, then $\tau_3 = \frac{\tau_{32}\times\tau_{31}}{\tau_{31}+\tau_{32}} = \tau_{32}\frac{1}{1+\frac{\tau_{32}}{\tau_{31}}} \approx \tau_{32}\frac{1}{1+0.039} \approx \tau_{32}$. A comparison between Figs. 3(a) and (b) shows that the ratio $\tau_{\mathrm{op}}/\tau_{21}$ has the maximum value 1.57×10^{-4}, then $\tau_2 = \frac{\tau_{\mathrm{op}}\times\tau_{21}}{\tau_{21}+\tau_{\mathrm{op}}} = \tau_{\mathrm{op}}\frac{1}{1+\frac{\tau_{\mathrm{op}}}{\tau_{21}}} \approx \tau_{\mathrm{op}}\frac{1}{1+1.57\times10^{-4}} \approx \tau_{\mathrm{op}}$. Under these considerations, the PIC of the QCL is $N_3 - N_2 \approx \frac{J}{eL_{\mathrm{a}}}\tau_{32}(1-\frac{\tau_{\mathrm{op}}}{\tau_{32}})$, and the ratio $\tau_{\mathrm{op}}/\tau_{32}$ has the maximum value 1.5×10^{-4} (Fig. 3). Then, we obtain

$$N_3 - N_2 \approx \frac{J}{eL_{\mathrm{a}}}\tau_{32}. \tag{13}$$

Thus, PIC can be simplified to Eq. (13). Assigning W_{W1}=3 nm, W_{W2}=14.15 nm, and W_{W3}=3 nm, τ_{32} has the maximum value, and the AR has the maximum population inversion (MPI). The corresponding LW is 46.44 μm, which is also the longest wavelength in Fig. 3(b), and the shortest one is 41.33 μm at W_{W1} = 1 nm, W_{W2} = 15.25 nm, and W_{W3} = 2.95 nm.

Figures 4(a) and 4(b) show the results when W_{W1} is set as the linear variable, W_{W3} is changed correspondingly, and W_{B4} is changed slightly by setting W_{B1} = 4 nm, W_{B2} = 1 nm, W_{W2} = 15.5 nm, and W_{B3} = 2 nm. The calculated values of W_{W1}, W_{W3}, and W_{B4} are listed in Table 2. Similar to Fig. 3, τ_{31} has the longest time among the three SELs, and τ_{31} changes from approximately 7.93 μs to 2.20 ms. As shown in Fig. 4, $\tau_{32}/\tau_{31} < 0.045$, $\tau_{\mathrm{op}}/\tau_{21} < 0.94\times10^{-4}$, and $\tau_{\mathrm{op}}/\tau_{32} < 0.98\times10^{-4}$. Hence, PIC can be also simplified to Eq. (13). The LW corresponding to the PIC is approximately 42.03 μm, which is

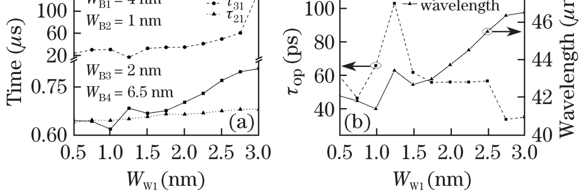

Fig. 3. (a) SELs τ_{32}, τ_{31}, and τ_{21} as functions of W_{W1}, W_{W2}, and W_{W3}. (b) POP SRT between subband2 and subband1 τ_{op} and LW of QCL as functions of W_{W1}, W_{W2}, and W_{W3}. W_{W1} is set as the linear variable shown in the horizontal coordinate, W_{W2} is changed correspondingly, and W_{W3} is changed slightly to make sure that $E_2–E_1 \approx E_{\mathrm{op}}$.

Table 1. Calculated Values of W_{W1}, W_{W2}, and W_{W3} Corresponding to Fig. 3.

Variable	W_{W1}	W_{W2}	W_{W3}
	0.50	15.50	3.00
	0.75	15.45	3.00
	1.00	15.25	2.95
	1.25	15.00	3.05
Value (nm)	1.75	14.90	2.95
	2.00	14.70	3.00
	2.25	14.55	3.00
	2.50	14.45	3.00
	2.75	14.30	3.00
	3.00	14.15	3.00

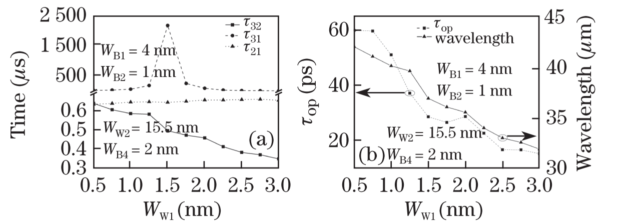

Fig. 4. (a) τ_{32}, τ_{31}, and τ_{21} as functions of W_{W1}, W_{W3}, and W_{B4}. (b) τ_{op} and LW of QCL as functions of W_{W1}, W_{W3}, and W_{B4}. W_{W1} is set as the linear variable shown in the horizontal coordinate, W_{W3} is changed correspondingly, and W_{B4} is changed slightly to make sure that $E_2–E_1 \approx E_{\mathrm{op}}$.

also the longest wavelength in Fig. 4 (b), and the shortest wavelength is 31.88 μm when W_{W1} = 3 nm, W_{W3} = 0.85 nm, and W_{B4} = 6.55 nm.

Setting W_{W2} as the linear variable, W_{W3} is changed correspondingly, and W_{B4} is changed slightly when W_{B1} = 4 nm, W_{W1} = 0.5 nm, W_{B2} = 1 nm, and W_{B3} = 2 nm. We obtain τ_{32}, τ_{31}, τ_{21}, and τ_{op}, and the LW is shown in Fig. 5. The calculated values of W_{W2}, W_{W3}, and W_{B4} are listed in Table 3. For all the calculated AR structures, despite the longest $\tau_{\mathrm{op}} \approx$1.78 ns, $\tau_{\mathrm{op}}/\tau_{21} < 0.28 \times 10^{-2}$ and $\tau_{\mathrm{op}}/\tau_{32} < 0.24 \times 10^{-2}$. Meanwhile, the ratio τ_{32}/τ_{31} changes as the structure of AR changes. For example, $\tau_{32}/\tau_{31} \approx 0.64$ at W_{W2} = 12 nm, W_{W3} = 4 nm, and W_{B4} = 6.4 nm, and $\tau_{32}/\tau_{31} \approx 1.88\times10^{-4}$ at W_{W2} = 16 nm, W_{W3} = 2.4 nm, and W_{B4} = 6.5 nm. Thus, τ_3 cannot be simply replaced by τ_{32}, and the PIC of the QCL becomes

$$N_3 - N_2 \approx \frac{J}{eL_{\mathrm{a}}}\tau_3. \tag{14}$$

By calculating τ_3, we find that the MPI about the structures of the AR in Fig. 5 is the structure when W_{W2} = 15 nm, W_{W3} = 3.3 nm, and W_{B4} = 6.5 nm, and that the corresponding LW is 44.93 μm, where the longest and shortest wavelengths are 46.27 and 25.89 μm, respectively.

The results in Fig. 6 are τ_{32}, τ_{31}, and τ_{21}, together with τ_{op} and LW as functions of W_{B3}, W_{W3}, and W_{W2}. Setting W_{B3} as the linear variable, W_{W3} is changed

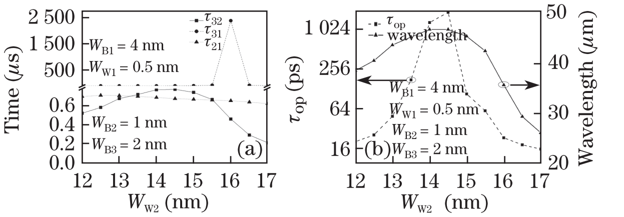

Fig. 5. (a) τ_{32}, τ_{31}, and τ_{21} as functions of W_{W2}, W_{W3}, and W_{B4}. (b) τ_{op} and LW of QCL as functions of W_{W2}, W_{W3}, and W_{B4}. W_{W3} is set as the linear variable shown in the horizontal coordinate, W_{W3} is changed correspondingly, and W_{B4} is changed slightly to make sure that E_2–E_1 $\approx$ E_{op}.

Table 2. Calculated Values of W_{W1}, W_{W3}, and W_{B4} Corresponding to Fig. 4.

Variable	W_{W1}	W_{W3}	W_{B4}
	0.50	3.00	6.50
	0.75	2.90	6.45
	1.00	2.80	6.55
	1.25	2.75	6.50
Value (nm)	1.50	2.45	6.50
	1.75	2.30	6.55
	2.00	2.20	6.55
	2.25	1.90	6.55
	2.50	1.65	6.55
	2.75	1.40	6.50
	3.00	0.85	6.55

correspondingly, and W_{W2} is changed slightly at W_{B1} = 4 nm, W_{W1} = 0.5 nm, W_{B2} = 1 nm, and W_{B4} = 6.5 nm. The calculated values of W_{B3}, W_{W3}, and W_{W2} are listed in Table 4. As shown in Fig. 6, for the calculated structures of AR, $\tau_{op}/\tau_{21} < 0.82 \times 10^{-2}$ and $\tau_{op}/\tau_{32} < 2.05 \times 10^{-3}$. τ_{32} may be longer than τ_{31} and reach 47.12 μs. The ratio τ_{32}/τ_{31} prominently changes so that the PIC of the QCL is also expressed as Eq. (14). The LW corresponding to the PIC is approximately 80 μm, and the longest and shortest wavelengths are 187.88 μm and 30.54 μm, respectively.

In Fig. 7, τ_{32}, τ_{31}, τ_{21}, τ_{op}, and LW of the QCL as functions of W_{B2} and W_{B4} were calculated by setting W_{B2} as the linear variable. Hence, W_{B4} is changed correspondingly at W_{B1} = 4 nm, W_{W1} = 0.5 nm, W_{W2} = 15.5 nm, W_{B3} = 2 nm, and W_{W3} = 3 nm. The calculated values of W_{B2} and W_{B4} are listed in Table 5. As shown in Fig. 7, $\tau_{op}/\tau_{21} < 0.75 \times 10^{-2}, \tau_{op}/\tau_{32} < 0.78 \times 10^{-3}$, and $\tau_{32}/\tau_{31} < 0.058$. Thus, the PIC of the QCL can be expressed as Eq. (13), and the MPI can be obtained when W_{B2} = 4 nm and W_{B4} = 6.55 nm, where the corresponding LW is 40.79 μm, and the longest and shortest wavelengths in Fig. 7(b) are 42.03 and 40.13 μm, respectively.

In conclusion, we analyze the QCL structures of $GaAs/Al_{0.15}Ga_{0.85}As$ and consider the ARs of the different widths of wells and barriers. We also discuss the PIC of the QCL. For some special cases, the PIC can be simplified and is proportional to the SEL between

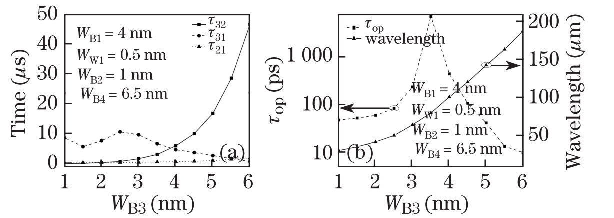

Fig. 6. (a) τ_{32}, τ_{31}, and τ_{21} as functions of W_{B3}, W_{W3}, and W_{W2}. (b) τ_{op} and LW of QCL as functions of W_{B3}, W_{W3}, and W_{W2}. W_{B3} is set as the linear variable shown in the horizontal coordinate, W_{W3} is changed correspondingly, and W_{W2} is changed slightly to make sure that E_2–E_1 $\approx$ E_{op}.

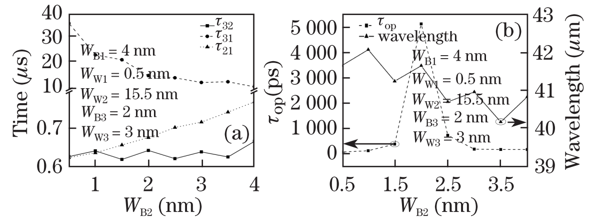

Fig. 7. (a) τ_{32}, τ_{31}, and τ_{21} as functions of W_{B2} and W_{B4}. (b) τ_{op} and LW of QCL as functions of W_{B2} and W_{B4}. W_{B2} is set as the linear variable shown in the horizontal coordinate, and W_{B4} is changed correspondingly to make sure that E_2–E_1 $\approx$ E_{op}.

Table 3. Calculated Values of W_{W2}, W_{W3}, and W_{B4} Corresponding to Fig. 5.

Variable	W_{W2}	W_{W3}	W_{B4}
	12.0	4.00	6.4
	12.5	3.90	6.5
	13.0	3.90	6.5
	13.5	3.80	6.5
	14.0	3.70	6.5
Value (nm)	14.5	3.70	6.5
	15.0	3.30	6.5
	15.5	3.00	6.5
	16.0	2.40	6.5
	16.5	1.50	6.5
	17.0	0.45	6.5

Table 4. Calculated Values of W_{B3}, W_{W3}, and W_{W2} Corresponding to Fig. 6.

Variable	W_{B3}	W_{W3}	W_{W2}
	1.0	2.35	15.45
	1.5	2.75	15.40
	2.0	3.00	15.50
	2.5	3.25	15.50
	3.0	3.55	15.45
Value (nm)	3.5	3.75	15.45
	4.0	3.90	15.50
	4.5	4.00	15.50
	5.0	4.00	15.50
	5.5	4.05	15.40
	6.0	4.15	15.50

Table 5. Calculated Values of W_{B2} and W_{B4} Corresponding to Fig. 7.

Variable	W_{B2}	W_{B4}
	0.50	6.65
	1.0	6.50
	1.5	6.50
	2.0	6.50
Value (nm)	2.5	6.60
	3.0	6.40
	3.5	6.50
	4.0	6.55

the second and the first excited states only, whereas some other cases imply that the PIC is proportional to the SL of the second excited states. Our results show the SELs between the states and the intersubband POP SRT between the second and the first subbands depend on the widths of the wells and barriers. Some optimal results are discussed in detail. The expressions of τ_{32}, τ_{31}, τ_{21}, τ_3, τ_2, τ_{op}, and PIC show the mechanism behind the obtained results. The changes in the widths of the QWs and barriers in AR lead to changes in the wave functions of the electron at different eigen states, which consequently cause changes in τ_{32}, τ_{31}, τ_{21}, τ_3, τ_2, and τ_{op}. Different PICs are obtained when different ARs are adopted.

This work was supported by the National Natural Science Foundation of China (No. 60976070) and the Special Funds of China Academy of Engineering Physics (No. 909).

References

1. R. Köhler, A. Tredicucci, F. Beltram, H. E. Beere, E. H. Linfield, A. G. Davies, D. A. Ritchie, R. C. Iotti, and F. Rossi, Nature **417,** 156 (2002).
2. B. S. Williams, Nat. Photon. **1,** 517 (2007).
3. R. Maulini, A. Lyakh, A. Tsekoun, R. Go, C. K. N. Patel, C. Pflügl, L. Diehl, and F. Capasso, Appl. Phys. Lett. **95,** 151112 (2009).
4. W. S. Holland, J. S. Greaves, B. Zuckerman, R. A. Webb, C. McCarthy, I. M. Coulson, D. M. Walther, W. R. F. Dent, Walter. K.Gear, and I. Robson, Nature **392,** 788 (1998).
5. T. Löfler, T. Bauer, K. J. Siebert, H. G. Roskos, A. Fitzgerald, and S. Czasch, Opt. Express **9,** 616 (2001).
6. Marco Califano, N. Q. Vinh, P. J. Phillips, Z. Ikonić R. W. Kelsall, P. Harrison, C. R. Pidgeon, B. N. Murdin, D. J. Paul, P. Townsend, J. Zhang, I. M. Ross, and A. G. Cullis, Phys. Rev. B **75,** 045338 (2007).
7. D. Graham-Rowe, Nat. Photon. **1,** 75 (2007).
8. T. Kubis, S. R. Mehrotra, and G. Klimeck, Appl. Phys. Lett. **97,** 261106 (2010).
9. E. J. Roan and S. L. Chuang, J. Appl. Phys. **69**, 3249 (1991).
10. P. Harrison, App. Phys. Lett. **75,** 2800 (1999).
11. J. H. Smet, C. G. Fonstad, and Q. Hu , J. Appl. Phys. **79,** 9305 (1996).
12. D. Ahnand S. L. Chuang, Phys. Rev. B **37,** 2579 (1998).